Control and Cybernetics

vol. **43** (2014) No. 2

Numerical simulations of Alfvén waves in the solar atmosphere with the PLUTO code

by

Piotr Wołoszkiewicz[1], Krzysztof Murawski[1], Zdzisław E. Musielak[2,3] and Andrea Mignone[4]

[1] Group of Astrophysics, Institute of Physics, UMCS, ul. Radziszewskiego 10, 20-031 Lublin, Poland; piotr.woloszkiewicz@gmail.com, kmur@kft.umcs.lublin.pl

[2] Department of Physics, University of Texas at Arlington, Arlington, TX 76019, USA; zmusielak@uta.edu

[3] Kiepenheuer-Institut für Sonnenphysik, Schöneckstr. 6, Freiburg; D–79104 Germany

[4] Dipartimento di Fisica Generale, Università di Torino, via Pietro Giuria 1, 10125 Torino, Italy; mignone@ph.unito.it

Abstract: With an adaptation of the PLUTO code, we present a 2.5-dimensional Cartesian magnetohydrodynamic model with the invariant ($\partial/\partial z = 0$) coordinate z of propagating magnetohydrodynamic-gravity waves in the solar atmosphere, permeated by curved magnetic field and constant gravity field $\mathbf{g} = -g\hat{\mathbf{y}}$. This code implements second-order accurate Godunov-type numerical scheme and MPI for high level of parallelization. We show that the inhomogeneous grid, originally built in the code, resolves well the system dynamics, resulting from the localized pulse initially launched in the transverse component of velocity V_z. We consider two cases for background magnetic field $\mathbf{B}_\mathrm{e} = [B_{\mathrm{e}x}, B_{\mathrm{e}y}, B_{\mathrm{e}z}]$ with its transverse component: (a) $B_{\mathrm{e}z} = 0$ and (b) $B_{\mathrm{e}z} \neq 0$. In case (a), the initial pulse triggers only Alfvén waves, described solely by V_z. These waves drive by ponderomotive forces the magnetoacoustic waves, associated with perturbations in V_x and V_y. As a result of $B_{\mathrm{e}z} \neq 0$, in the (b) case, Alfvén waves are coupled to their magnetoacoustic counterparts and all three velocity components are perturbed. We show that in this case the PLUTO code is accurate, its order being 1.97 and the numerically induced flow is of magnitude ≈ 0.1 km s^{-1}, i.e. by a factor of at least $\approx 10^3$ lower than the characteristic (Alfvén) speed of the system. The errors, associated with the selenoidal condition, are low with the max $|\nabla \cdot \mathbf{B}| \approx 1.3 \cdot 10^{-10}$ Tesla km^{-1}. We conclude that the PLUTO code copes well with resolving all spatial and temporal scales that appear in this numerically challenging system.

Keywords: MHD, Alfvén waves

1. Introduction

Recent observational and theoretical results indicate that Alfvén waves are present in the solar atmosphere (see, e.g. Banerjee et al., 2007; Chmielewski et al., 2013). As Alfvén waves are incompressible, they are difficult do detect, yet several reports of their presence in the solar atmosphere were published, based on observational data provided by contemporary space missions, such as TRACE and SDO (see, e.g., Banerjee et al., 2007; Tomczyk et al., 2007; De Pontieu et al., 2007). Alfvén waves require magnetic fields, whose tension is the restoring force for these waves. Observations revealed that the solar atmosphere is permeated by magnetic fields, which are organized in various structures such as flux-tubes and coronal arcades. According to a traditional view, Alfvén waves can be excited in lower dynamic layers of the solar atmosphere. These waves carry their energy into overlaying regions, significantly contributing to their heating.

The study of the injection and propagation of Alfvén waves into the solar corona from the photosphere is an important problem in solar physics, motivated by recent satellite observations of these waves, and by the unresolved question of corona heating and acceleration of the solar wind, where these waves can provide the required energy and momentum input (see Ofman, 2010). Extensive theoretical studies of Alfvén waves in the solar atmosphere were performed in the past. Among others, Murawski and Musielak (2010) considered Alfvén waves in the solar atmosphere, showing that as the result of cut-off frequencies, these waves are not able to propagate freely into the upper regions of the solar atmosphere, undergoing reflection towards lower layers. While studying the impulsively triggered Alfvén waves in the solar atmosphere, Chmielewski et al. (2013) concluded that they may result in the observed non-thermal broadening of some spectral lines in solar coronal holes. The nonlinear wave equations were derived for magnetoacoustic waves driven by ponderomotive forces associated with Alfvén waves (see Murawski, 1992; Nakariakov, Roberts and Murawski, 1997, 1998). Gruszecki et al. (2007) showed that Alfvén waves are attenuated by energy leakage into the ambient plasma as a result of curved magnetic lines. A number of papers have been published on the modelling and propagation of the Alfvén waves from the photosphere into the corona in 1.5D (see, e.g., Kudoh and Shibata, 1999; Suzuki and Inutsuka, 2006; Suzuki, 2007; Matsumoto and Shibata, 2010), in 2.5D (see, e.g. Fedun et al., 2011; Matsumoto and Suzuki, 2012), and 3D (see, e.g., Vigeesh et al., 2012). Chmielewski et al. (2014) discussed Alfvén wave propagation in a solar corona arcade, but they did not consider coupling between Alfvén and magnetoacoustic waves, which is the subject of this paper.

We study Alfvén-magnetoacoustic waves coupling in the gravitationally stratified solar atmosphere by solving numerically the time-dependent magnetohydrodynamic equations with a realistic temperature distribution. This paper is

organized as follows. Section 2 presents the numerical model we devised. In Section 3, we describe briefly the PLUTO code, and in Section 4, we show some numerical experiments performed. We conclude this paper with the presentation of our main numerical results.

2. Numerical model

We consider a gravitationally-stratified solar atmosphere that is described by the ideal MHD equations:

$$\frac{\partial}{\partial t}\begin{pmatrix} \varrho \\ \varrho\mathbf{v} \\ E \\ \mathbf{B} \end{pmatrix} + \nabla\cdot\begin{pmatrix} \varrho\mathbf{v} \\ \varrho\mathbf{v}\mathbf{v} - \dfrac{\mathbf{B}\mathbf{B}}{\mu} + \mathbf{I}p_t \\ (E+p_t)\mathbf{v} - \dfrac{\mathbf{B}}{\mu}(\mathbf{v}\cdot\mathbf{B}) \\ \mathbf{v}\mathbf{B} - \mathbf{B}\mathbf{v} \end{pmatrix} = \begin{pmatrix} 0 \\ \varrho\mathbf{g} \\ \varrho\mathbf{v}\cdot\mathbf{g} \\ \mathbf{0} \end{pmatrix}. \tag{1}$$

Here, the symbol ϱ denotes mass density, $\mathbf{v}$ is the velocity, $p_t = p + \mathbf{B}^2/(2\mu)$ is the total (thermal + magnetic) pressure, $\mathbf{B}$ is the magnetic field such that $\nabla\cdot\mathbf{B} = 0$, μ is the magnetic permeability, $\mathbf{I}$ is the unit matrix, and E is the total energy density (the sum of the internal, kinetic, and magnetic energy densities), viz.

$$E = \frac{p}{\gamma - 1} + \frac{\varrho\mathbf{v}^2}{2} + \frac{\mathbf{B}^2}{2\mu} \tag{2}$$

with $\gamma = 5/3$ being the specific heats ratio. The system (1) is closed by the ideal gas law

$$p = \frac{k_\mathrm{B}}{\hat{m}}\varrho T\ . \tag{3}$$

In this expression, T denotes temperature, k_B is the Boltzmann constant, and $\hat{m}$ is the mean particle mass. We specify $\hat{m}$ by the mean mass equal 0.6, which is typical value for the solar corona. The source terms on the right hand side of Eq. (1) include contributions from gravity $\mathbf{g} = [0, -g, 0]$ with its magnitude $g = 274$ m s^{-2}. The use of constant gravity is only applicable close to the photosphere. In Eq. (1) we neglected non-ideal (plasma viscosity, magnetic diffusivity, thermal conduction) and non-adiabatic (cooling/heating) effects. The former (latter) are expected to be important in strong spatial gradients such as those occurring at the transition region (at low atmosphere layers). However, these effects modify the amplitude of the MHD waves and therefore they are not expected to alter the qualitative behaviour of the system. We plan to include these effects in our future studies.

2.1. Numerical model of the solar atmosphere

2.1.1. Equilibrium

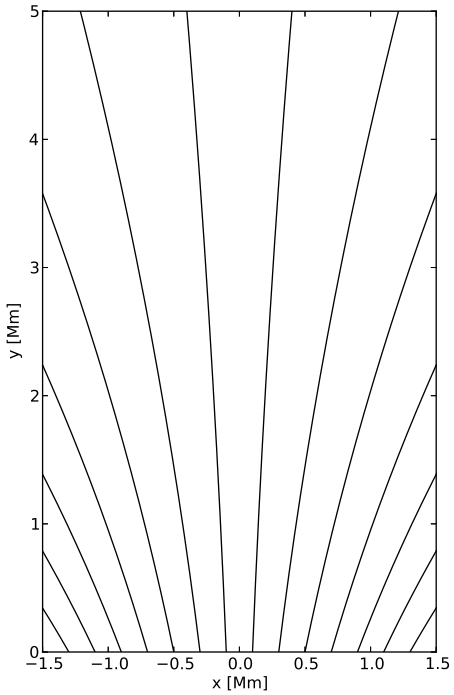

Figure 1. Equilibrium magnetic field lines in the solar atmosphere

In the numerical model we devise, we assume that z is an invariant coordinate such as $\partial/\partial z = 0$ but allow the z-components of velocity, V_z, and magnetic field, B_z, to vary with x and y. The solar atmosphere is in static equilibrium ($\mathbf{V}_\mathrm{e} = \mathbf{0}$) with current-free (and therefore force-free) magnetic field, i.e.

$$\nabla \times \mathbf{B}_\mathrm{e} = \mathbf{0}\,, \qquad (\nabla \times \mathbf{B}_\mathrm{e}) \times \mathbf{B}_\mathrm{e} = \mathbf{0}\,. \tag{4}$$

Henceforth, the subscript $_e$ corresponds to equilibrium quantities. As a result of Eq. (4) we determine the magnetic field as

$$\mathbf{B}_\mathrm{e}(x,y) = [B_{ex}, B_{ey}, B_{ez}] = \nabla \times (A_\mathrm{e}\hat{\mathbf{z}}) + B_{ez}\hat{\mathbf{z}}\,, \tag{5}$$

where $\hat{\mathbf{z}}$ is the unit vector along the z-direction and the magnetic flux function is

$$A_\mathrm{e}(x,y) = \frac{x(y_\mathrm{ref}-b)^2}{x^2+(y-b)^2} B_\mathrm{ref}\,. \tag{6}$$

We set and hold fixed the vertical coordinate of the magnetic pole, $b = -5$ Mm, and the reference level, $y_{\rm ref} = 10$ Mm. We choose $B_{\rm ref}$ by requiring that the Alfvén speed,

$$c_{\rm A}(x,y) = \sqrt{\frac{B_{ex}^2 + B_{ey}^2}{\mu \varrho_{\rm e}(y)}}\,, \tag{7}$$

and sound speed,

$$c_{\rm s}(y) = \sqrt{\frac{\gamma p_{\rm e}(y)}{\varrho_{\rm e}(y)}}\,, \tag{8}$$

satisfy the following constraint: $c_{\rm A}(0, y_{\rm ref}) = 10\; c_{\rm s}(y_{\rm ref})$. The equilibrium magnetic field lines, which are described by Eq. (5), are presented in Fig. 1. Note that magnetic field lines diverge with height. This magnetic field models solar coronal structures and the non-active region in the solar photosphere.

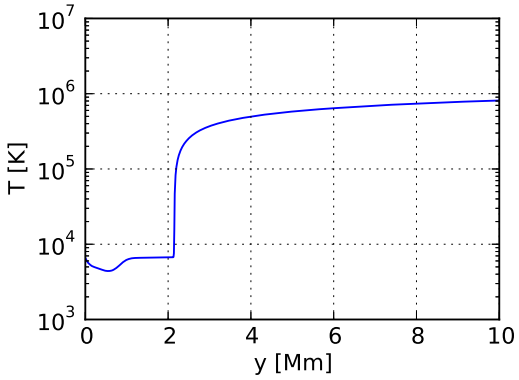

Figure 2. Equilibrium profile of temperature $T_{\rm e}(y)$ in the solar atmosphere

As a result of Eq. (4), the pressure gradient has to be balanced by the gravity force,

$$-\nabla p_{\rm e} + \varrho_{\rm e}\mathbf{g} = \mathbf{0}\,. \tag{9}$$

Using the ideal gas law of Eq. (3) and the y-component of the hydrostatic pressure balance, indicated by Eq. (9), we express the equilibrium gas pressure and the mass density as

$$p_{\rm e}(y) = p_{\rm ref} \exp\left(-\int_{y_{\rm ref}}^{y} \frac{dy'}{\Lambda(y')}\right)\,, \qquad \varrho_{\rm e}(y) = \frac{p_{\rm e}(y)}{g\Lambda(y)}\,, \tag{10}$$

where

$$\Lambda(y) = \frac{k_B T_{\rm e}(y)}{\hat{m} g} \tag{11}$$

is the pressure scale-height, and $p_{\rm ref}$ denotes the gas pressure at the reference level, $y_{\rm ref}$.

We adopt a realistic model of the plasma temperature profile that was derived by Avrett and Loeser (2008). This profile is displayed in Fig. 2, which reveals that $T_{\rm e}(y)$ falls off with height up to $y \approx 0.5$ Mm, where $T_{\rm e}$ attains its minimum of about 4400 K. Higher up, $T_{\rm e}(y)$ grows with y and displays an abrupt rise at the transition region, located at $y \approx 2.1$ Mm. Yet higher up, in the solar corona, $T_{\rm e}(y)$ settles at about the value of 1 MK. The temperature profile determines uniquely the equilibrium mass density $\varrho_{\rm e}(y)$ and the gas pressure $p_{\rm e}(y)$ profiles, which are obtained by means of equation (10). These profiles are displayed in Fig. 3, which shows that $p_{\rm e}(y)$ and $\varrho_{\rm e}(y)$ fall off with altitude.

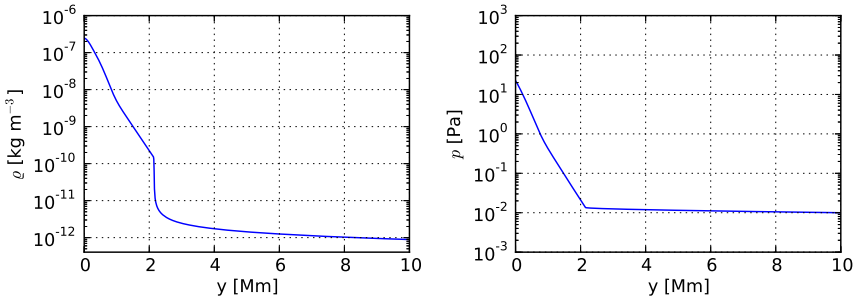

Figure 3. Equilibrium profiles of mass density $\varrho_{\rm e}$ (left) and gas pressure $p_{\rm e}$ (right) vs. height in the solar atmosphere

2.1.2. Perturbations

At $t = 0$ s we perturb the model equilibrium (described in Section 2.1.1) by the initial pulse in the z-component of velocity, which is expressed as follows:

$$V_z(x,y) = A_V \times \frac{x - x_0}{w} \times \exp\left(-\frac{(x-x_0)^2 + (y-y_0)^2}{w^2}\right), \tag{12}$$

where (x_0, y_0) is initial position of the pulse, w is its width, and A_V specifies its amplitude. We set and hold fixed ($x_0 = 0$, $y_0 = 1.6$) Mm, $w = 0.05$ Mm, and $A_V = 0.25$ Mm s^{-1}. The latter value results in the effective pulse amplitude of about 0.1 Mm s^{-1}. The pulse of Eq. (12) would mimic a twist in 3D, which corresponds to Alfvén waves.

3. The PLUTO code

PLUTO is a finite-volume/finite-difference code (see Mignone et al., 2007, 2012), that is designed to integrate numerically a system of conservation laws

$$\frac{\partial \mathbf{U}}{\partial t} + \nabla \cdot \mathcal{T}(\mathbf{U}) = \mathcal{S}(\mathbf{U}), \tag{13}$$

where $\mathbf{U}$ represents a set of conservative quantities, $\mathcal{T}(\mathbf{U})$ is the flux tensor, and $\mathcal{S}(\mathbf{U})$ defines the source terms.

PLUTO adopts a structured mesh approach for the solution of the system of conservation laws (13). Flow quantities are discretized on a logically rectangular computational mesh enclosed by a boundary and augmented with ghost cells in which boundary conditions are implemented. For all considered cases we set the simulation box as (-1,1) Mm × (1,7) Mm, meaning that a 2 Mm (6 Mm) span along the horizontal (vertical) direction is imposed. The extent of the simulation box in the y-direction ensures that we catch the essential physics occurring in the solar atmosphere. We impose the boundary conditions by fixing in there all plasma quantities at all four boundaries to their equilibrium values. Computations are done using double precision arithmetic with the use of MPI (see Mignone et al., 2007). The required number of processors was 24 and we used 1.2 hours of CPU time for this calculation. For the present application we adopted a static uniform grid. Along the x-direction this grid is divided into 800, while in y-direction into 2400 equal cells.

In our problem, we set the Courant-Friedrichs-Lewy number equal to 0.8 and choose piecewise TVD linear interpolation in MUSCL-Hancock scheme, which leads to 2$^{\text{nd}}$ order accuracy in space, and adopt the Harten-Lax-van Leer Discontinuities (HLLD) approximate Riemann solver.

4. Results of numerical simulations

4.1. Error analysis

Figure 4 illustrates the numerically induced flow in the case when no initial pulse ($A_V = 0$ in Eq. 12) was launched in the system. It is discernible that the flow magnitude is of the order of ≈ 0.1 km s^{-1}, which is much lower than the characteristic sound, $c_{\rm s} = \sqrt{\gamma p_{\rm e}/\varrho_{\rm e}} \approx 0.1$ Mm s^{-1}, and Alfvén, $c_{\rm A} = |B_{\rm e}|\sqrt{\mu\varrho_{\rm e}} \approx 1$ Mm s^{-1}, speeds.

We perform now the error analysis in order to verify that the obtained numerical results do not suffer from excessive numerical errors, which can be quantized by the following formula:

$$\text{Error} = \sum_{\rm ij} \Delta x \Delta y |V_{\rm ij}| \,. \tag{14}$$

Figure 5 illustrates the results of a mesh refinement study for the case of $B_{\rm ez} = 0$ and the initial pulse-free ($A_V = 0$) structure. The numerically induced flow is evaluated on a sequence of different grids, and the norm of the error is plotted as a function of Δx, while the grid along y remains fixed.

Figure 5 shows the errors at four moments of time. Note that as a result of growing numerically the induced flow, the error grows in time. Yet, it becomes smaller for a finer grid size Δx.
With the use of the following formula:

$$log|\text{Error}| \approx const + a\, log|\Delta x| \tag{15}$$

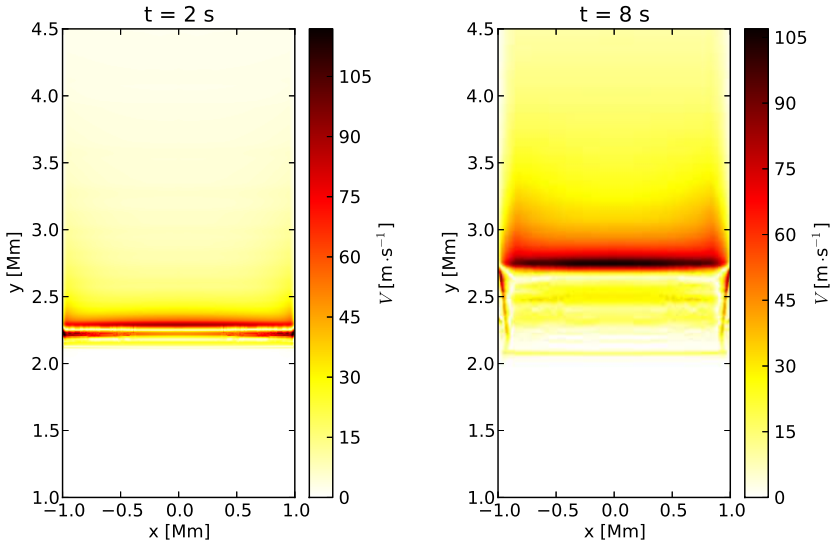

Figure 4. Spatial profiles of spurious flow $\sqrt{V_{\rm x}^2 + V_{\rm y}^2}$ at $t = 2$ s (left) and $t = 8$ s (right) for the case of $B_{ez} = B_{\rm ref}$ and initial pulse-free system, $A_V = 0$ in Eq. (12)

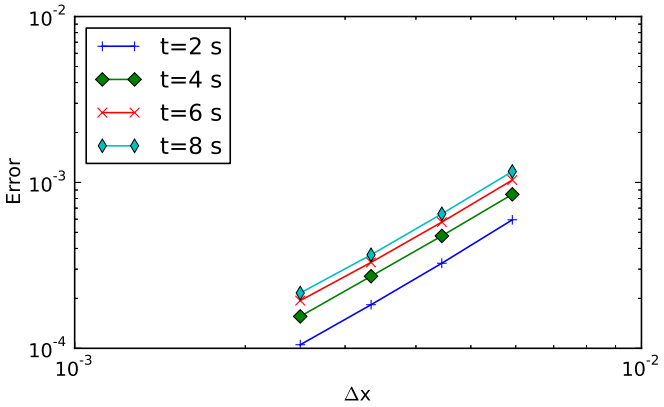

Figure 5. Log-log plot of the error (ℓ^1-norm) vs. grid size at four different instants of time t

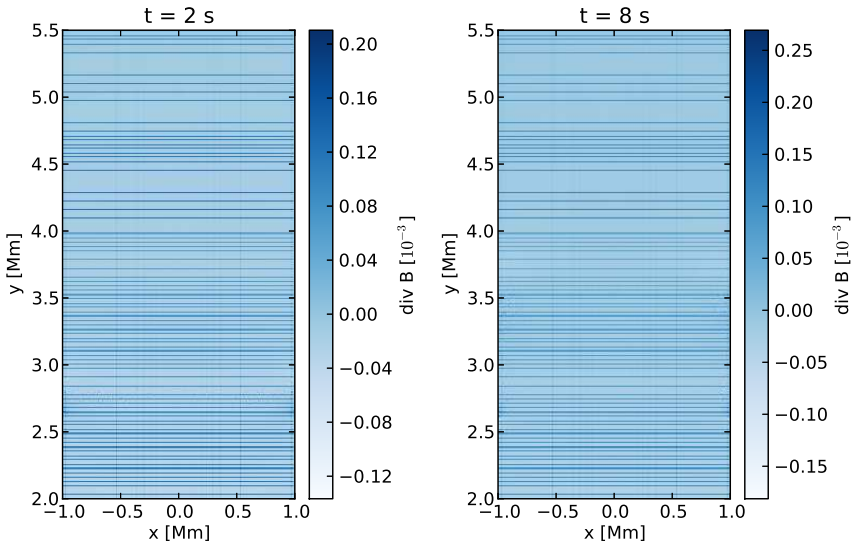

Figure 6. Spatial profiles of $\nabla \cdot \mathbf{B}$ at $t = 2$ s (left) and $t = 8$ s (right) for the case of $B_{ez} = B_{\rm ref}$ and no pulse in the system, $A_V = 0$ in Eq. (12)

we find the observed order of accuracy, $a = 1.97$, which is very close to the theoretical order of accuracy 2.

Finally, we verify that numerical errors associated with non-zero $\nabla \cdot \mathbf{B}$ are very small. Indeed, Fig. 6 displays spatial profiles of $\nabla \cdot \mathbf{B}$ at two consecutive moments of time. We conclude from this figure that the magnitude of $\nabla \cdot \mathbf{B}$ is of the order of 10^{-10} T km^{-1} and its average value is $3.5 \cdot 10^{-12}$ T km^{-1}, which is very low.

4.2. The case of $B_{ez} = 0$

In the case of $B_{ez} = 0$ the transverse component of velocity $V_z(x, y)$, corresponding to Alfvén waves as in the linear limit, small amplitude waves, are described by the wave equation (see Murawski and Musielak, 2010)

$$\frac{\partial^2 V_z}{\partial t^2} - c_{\rm A}^2(x, y)\frac{\partial^2 V_z}{\partial s^2} = 0 \,, \tag{16}$$

where s is the coordinate along magnetic field lines. The x- and y-components of velocity, V_x, V_y, describe magnetoacoustic waves which are coupled (see Murawski, 2002). In a strongly magnetized plasma, such as in the solar corona, the coupling is weak and V_x describes essentially fast magnetoacoustic waves, while V_y is associated with slow magnetoacoustic waves, which are affected by the gravity.

Figure 7 shows the spatial profiles of $V_z(x, y, t)$ at four moments of time. The initial pulse spreads into two counter-propagating Alfvén waves, which are

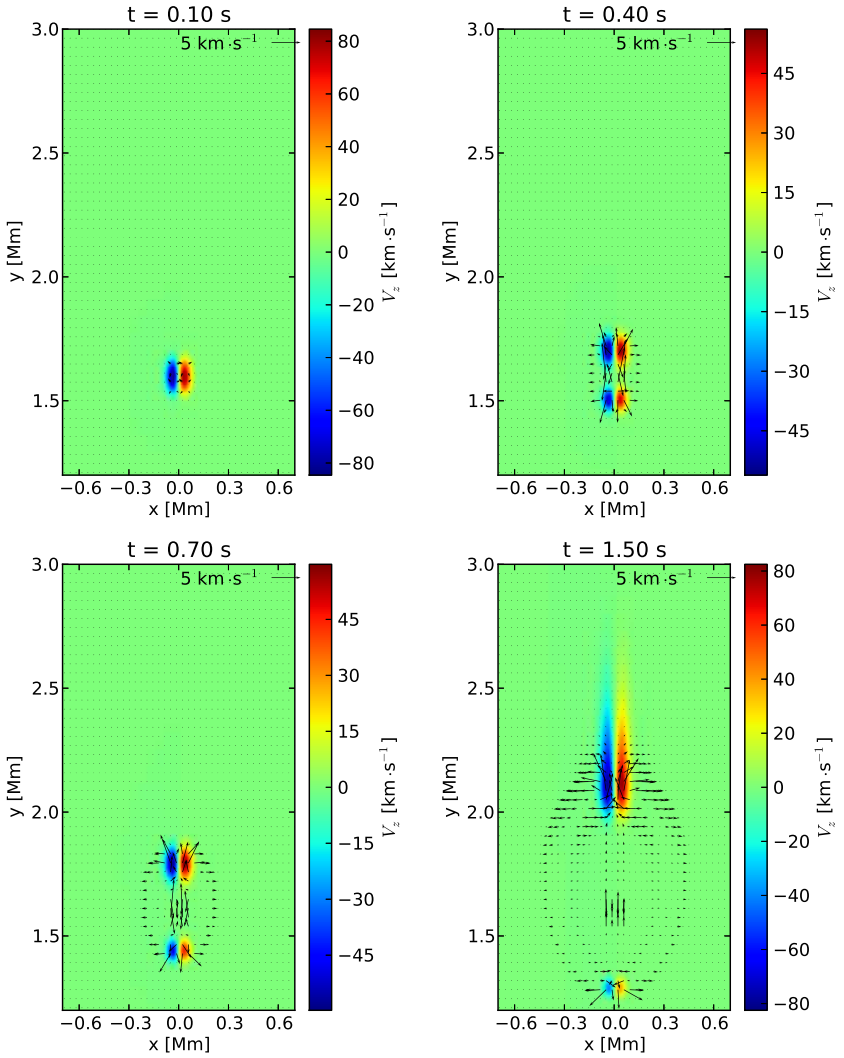

Figure 7. Spatial profiles of $V_z(x, y)$ and (V_x, V_y) (arrows) at $t = 0.1$ s (left-top), $t = 0.4$ s (right-top), $t = 0.7$ s (left-bottom) and $t = 1.5$ s (right-bottom) for the case of $B_{ez} = 0$

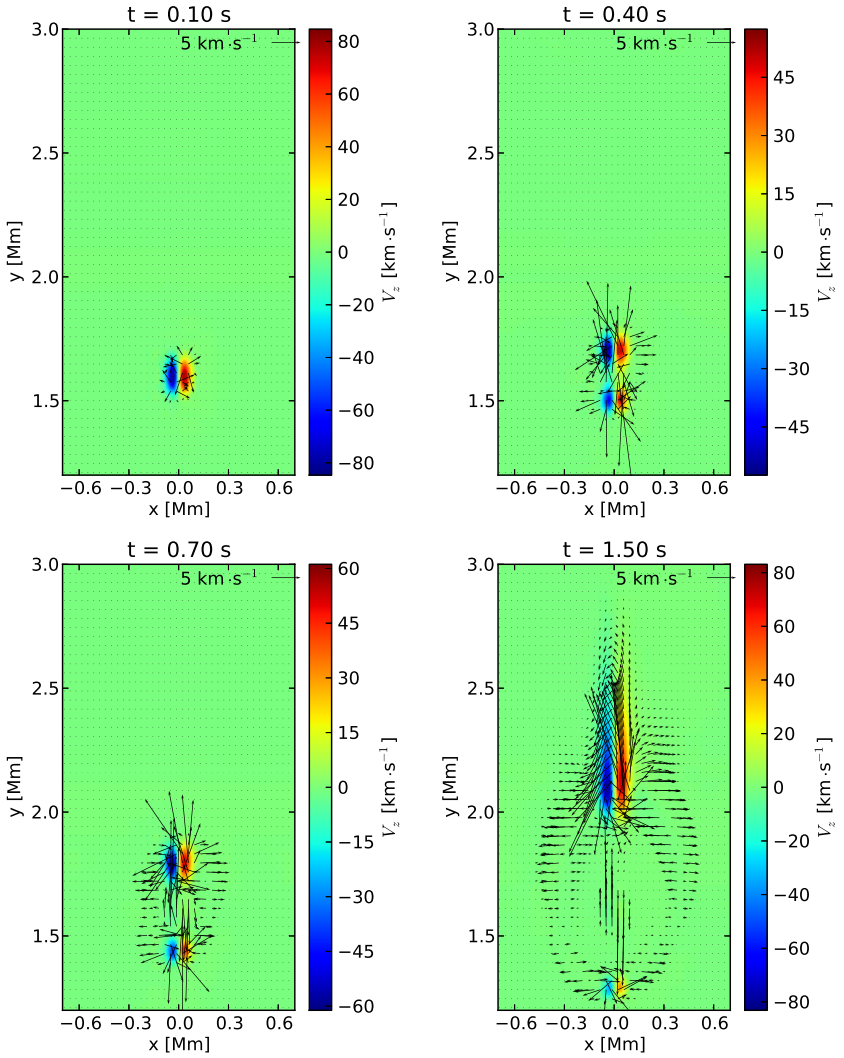

Figure 8. Spatial profiles of $V_z(x, y)$ and (V_x, V_y) (arrows) at $t = 0.1$ s (left-top), $t = 0.4$ s (right-top), $t = 0.7$ s (left-bottom) and $t = 1.5$ s (right-bottom) for the case of $B_{ez} = B_{\rm ref}$

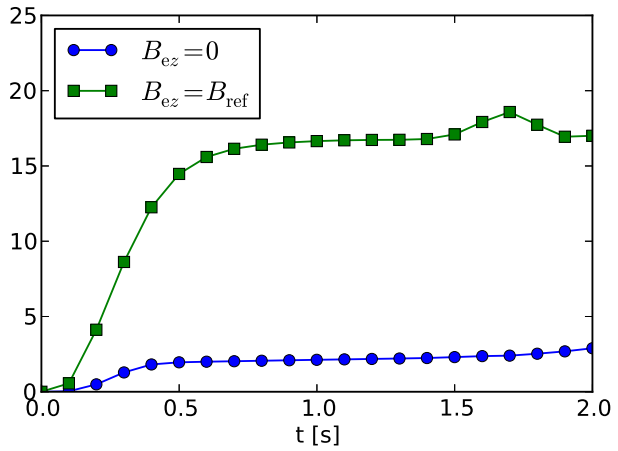

Figure 9. Total kinetic energy (in normalized units) of magnetoacoustic waves for different instants of time

already seen at $t = 0.1$ s (left-top). These waves propagate along magnetic field lines with a local Alfvén speed. As this speed is lower for lower values of y, the downward propagating Alfvén waves move slower than their upward propagating counterparts. As a result of that, the upward propagating Alfvén waves cover longer distance than the downward moving waves. At $t = 0.4$ s the upward moving waves reached the altitude of $y \approx 1.75$ Mm while the downward propagating waves covered about twice smaller distance (top-right). At $t = 1.5$ s the upward moving waves already reached the transition region and entered the solar corona (left-bottom). Some Alfvén waves are subject to reflection from the transition region. This effect is discernible at $t = 1.5$ s (right-bottom). With Alfvén waves some magnetoacoustic waves are seen. These waves are driven by Alfvén waves through the ponderomotive forces, which are associated with spatial gradients of magnetic pressure, and they are represented by the arrows in Fig. 7.

4.3. The case of $B_{ez} \neq 0$

In the case of $B_{ez} \neq 0$ the linear Alfvén waves are linearly coupled to the magnetoacoustic waves and these waves correspond to all velocity components. Figure 8 illustrates spatial profiles of the transversal component of velocity V_z and velocity vectors (V_x, V_y). Comparing this figure to Fig. 7 we see much more of the signal associated with V_x and V_y. This is a consequence of the Alfvén-magnetoacoustic waves coupling resulting from $B_{ez} \neq 0$. The initial pulse excites all MHD waves which are later on affected by the constant gravity field.

Figure 9 displays the kinetic energy

$$E_{\mathrm{m-w}}(t) = \frac{1}{2}\sum_{\mathrm{ij}} \Delta x \Delta y \varrho_{\mathrm{ij}} (V^2_{x,\mathrm{ij}} + V^2_{y,\mathrm{ij}}) \; . \tag{17}$$

It is discernible that $E_{\mathrm{m-w}}$ is much larger in the case of $B_{\mathrm{ez}} > 0$ (Fig. 9, top curve) which results from much more flow $[V_{\mathrm{x}}, V_{\mathrm{y}}]$ being generated due to coupling between Alfvén and magnetoacoustic waves.

5. Summary

We performed numerical simulations of Alfvén and magnetoacoustic waves in a magnetically structured and gravitationally stratified solar atmosphere, which is specified by the realistic temperature profile (see Avrett and Loeser, 2008). The curved magnetic field that satisfies the current-free condition was devised by Konkol, Murawski and Zaqarashvili (2012). This magnetic field is supplemented by a uniform transversal component, $B_{\mathrm{e}z}$.

The results of our simulations are summarized as follows. The initial pulse that is launched in the transversal velocity triggers Alfvén waves in the case of $B_{\mathrm{e}z} = 0$. These waves propagate along magnetic field lines in agreement with theoretical findings (see Murawski and Musielak, 2010). Finite-amplitude Alfvén waves drive through ponderomotive forces magnetoacoustic waves that are affected by the gravity. In the case of $B_{\mathrm{e}z} \neq 0$, the initial pulse excites all MHD-gravity waves and Alfvén waves are coupled to magnetoacoustic waves.

The solar atmosphere is stratified by the gravity and a strong, curved magnetic field, this posing a formidable task for numerical simulations. Notwithstanding this, we showed that the numerical errors are of small magnitude, and the PLUTO code is a good numerical tool to simulate MHD waves in the solar atmosphere. In particular, we showed that the numerically induced flow is of the order of 0.1 km s^{-1}, which is by a factor of at least $\approx 10^3$ lower than the characteristic speeds of the system. As a result of this flow the accuracy of the PLUTO code is slightly reduced from its theoretical value 2 to 1.97. We have also verified that $|\nabla \cdot \mathbf{B}/(B_0/L_0)| \approx 10^{-10}$, which is very close to its expected value of 0. Here, $B_0 = 10^{-3}$ Tesla is the typical magnitude of the magnetic field and $L_0 = 1$ Mm is the typical length scale. We conclude that the PLUTO code copes well with resolving all spatial and temporal scales in this very numerically challenging system. The paper demonstrates that the PLUTO code works well and that its numerical results are encouraging.

This work has been supported by NSF under the grant AGS 1246074 (Krzysztof Murawski and Zdzisław E. Musielak), and by the Alexander von Humboldt Foundation (Zdzisław E. Musielak). This research was carried out with the support of the HPC Infrastructure for Grand Challenges of Science and Engineering Project, co-financed by the European Regional Development Fund under the Innovative Economy Operational Program (Piotr Woloszkiewicz and Krzysztof Murawski).

References

Avrett, E. H., and Loeser, R. (2008) Models of the Solar Chromosphere and Transition Region from SUMER and HRTS Observations: Formation of the Extreme-Ultraviolet Spectrum of Hydrogen, Carbon, and Oxygen. *Astrophysical Journal, Supplement* **175**, 229-276.

Banerjee, D., Erdélyi, R., Oliver, R., and O'Shea, E. (2007) Present and Future Observing Trends in Atmospheric Magnetoseismology. *Sol. Phys.* **246**, 3-29.

Chmielewski, P., Murawski, K., Musielak, Z. E., and Srivastava, A. K. (2014) Numerical simulation of impulsively generated Alfvén waves in solar magnetic arcades. *Astrophysical Journal, Supplement*, submitted.

Chmielewski, P., Srivastava, A. K., Murawski, K., and Musielak, Z. E. (2013) Pulse-driven non-linear Alfvén waves and their role in the spectral line broadening. *Monthly Notices of the Royal Astronomical Society* **428**, 40-49.

De Pontieu, B., McIntosh, S. W., Carlsson, M., Hansteen, V. H., Tarbell, T. D., Schrijver, C. J., Title, A. M., Shine, R. A., Tsuneta, S., Katsukawa, Y., Ichimoto, K., Suematsu, Y., Shimizu, T., and Nagata, S. (2007) Chromospheric Alfvénic Waves Strong Enough to Power the Solar Wind. *Science* **318**, 1574.

Fedun, V., Verth, G., Jess, D. B., and Erdélyi, R. (2011) Frequency Filtering of Torsional Alfvén Waves by Chromospheric Magnetic Field. *Astrophysical Journal, Letters* **740**, L46.

Gruszecki, M., Murawski, K., Solanki, S. K., and Ofman, L. (2007) Attenuation of Alfvén waves in straight and curved coronal slabs. *Astronomy and Astrophysics* **469**, 1117-1121.

Konkol, P., Murawski, K., and Zaqarashvili, T. V. (2012) Numerical simulations of magnetoacoustic oscillations in a gravitationally stratified solar corona. *Astronomy and Astrophysics* **537**, A96.

Kudoh, T., and Shibata, K. (1999) Alfvén Wave Model of Spicules and Coronal Heating. *Astrophysical Journal* **514**, 493-505.

Matsumoto, T., and Shibata, K. (2010) Nonlinear Propagation of Alfvén Waves Driven by Observed Photospheric Motions: Application to the Coronal Heating and Spicule Formation. *Astrophysical Journal* **710**, 1857-1867.

Matsumoto, T., and Suzuki, T. K. (2012) Connecting the Sun and the Solar Wind: The First 2.5-dimensional Self-consistent MHD Simulation under the Alfvén Wave Scenario. *Astrophysical Journal* **749**, 8.

Mignone, A., Bodo, G., Massaglia, S., Matsakos, T., Tesileanu, O., Zanni, C., and Ferrari, A. (2007) PLUTO: a Numerical Code for Computational Astrophysics. *Astrophysical Journal, Suplement Series* **170**, 1, 228–234.

Mignone, A., Zanni, C., Tzeferacos, P., van Straalen, B., Colella, P., and Bodo, G. (2012) The PLUTO Code for Adaptive Mesh Computations in Astrophysical Fluid Dynamics. *Astrophysical Journal, Supplement*

198, 7.

Murawski, K. (1992) Alfven-magnetosonic waves interaction in the solar corona. *Sol. Phys.* **139**, 279-297.

Murawski, K. (2002) Analytical and numerical methods for wave propagation in fluid media. *World Scientific* **175**, 645.

Murawski, K., and Musielak, Z. E. (2010) Linear Alfvén waves in the solar atmosphere. *Astronomy and Astrophysics* **518**, A37.

Nakariakov, V. M., Roberts, B., and Murawski, K. (1997) Alfven Wave Phase Mixing as a Source of Fast Magnetosonic Waves. *Sol. Phys.* **175**, 93-105.

Nakariakov, V. M., Roberts, B., and Murawski, K. (1998) Nonlinear coupling of MHD waves in inhomogeneous steady flows. *Astronomy and Astrophysics* **332**, 795-804.

Ofman, L. (2010) Wave Modeling of the Solar Wind. *Living Reviews in Solar Physics* **7**, 4.

Suzuki, T. K. (2007) Self-Consistent MHD Modeling of Solar Wind. *New Solar Physics with Solar-B Mission **369** of Astronomical Society of the Pacific Conference Series*, 557.

Suzuki, T. K., and Inutsuka, S.-I. (2006) Solar winds driven by nonlinear low-frequency Alfvén waves from the photosphere: Parametric study for fast/slow winds and disappearance of solar winds. *Journal of Geophysical Research (Space Physics)* **111**, 6101.

Tomczyk, S., McIntosh, S. W., Keil, S. L., Judge, P. G., Schad, T., Seeley, D. H., and Edmondson, J. (2007) Alfvén Waves in the Solar Corona. *Science* **317**, 1192.

Vigeesh, G., Fedun, V., Hasan, S. S., and Erdélyi, R. (2012) Three-dimensional Simulations of Magnetohydrodynamic Waves in Magnetized Solar Atmosphere. *Astrophysical Journal* **755**, 18.